HHS Public Access

Author manuscript

Eur J Radiol. Author manuscript; available in PMC 2024 November 01.

Published in final edited form as:

Eur J Radiol. 2023 November ; 168: 111095. doi:10.1016/j.ejrad.2023.111095.

Evaluation of a Deep Learning-based Algorithm for Post-Radiotherapy Prostate Cancer Local Recurrence Detection Using Biparametric MRI

Enis C. Yilmaz, MD[1], **Stephanie A. Harmon, PhD**[1], **Mason J. Belue, BS**[1], **Katie M. Merriman, BS**[1], **Tim E. Phelps, PhD**[1], **Yue Lin, BS**[1], **Charisse Garcia, RN**[2], **Lindsey Hazen, RN**[2], **Krishnan R. Patel, MD**[3], **Maria J. Merino**[4], **Bradford J. Wood, MD**[2], **Peter L. Choyke, MD**[1], **Peter A. Pinto, MD**[5], **Deborah E. Citrin, MD**[3,*], **Baris Turkbey, MD**[1,6,*]

[1]Molecular Imaging Branch, National Cancer Institute, National Institutes of Health, Bethesda, MD (E.C.Y., S.A.H., M.J.B., K.M.M., T.E.P., Y.L., P.L.C., B.T.)

[2]Center for Interventional Oncology (C.G., L.H., B.J.W.), National Cancer Institute, National Institutes of Health, Bethesda, Maryland; Department of Radiology (B.J.W.), Clinical Center, National Institutes of Health, Bethesda, Maryland

[3]Radiation Oncology Branch (K.R.P., D.E.C.), National Cancer Institute, National Institutes of Health, Bethesda, Maryland

[4]Laboratory of Pathology (M.J.M.), National Cancer Institute, National Institutes of Health, Bethesda, Maryland

[5]Urologic Oncology Branch (P.A.P.), National Cancer Institute, National Institutes of Health, Bethesda, Maryland

[6]Molecular Imaging Branch (B.T.), National Cancer Institute, National Institutes of Health, 10 Center Dr., MSC 1182, Building 10, Room B3B85, Bethesda, Maryland

Abstract

Objective: To evaluate a biparametric MRI (bpMRI)-based artificial intelligence (AI) model for the detection of local prostate cancer (PCa) recurrence in patients with radiotherapy history.

Materials and Methods: This study included post-radiotherapy patients undergoing multiparametric MRI and subsequent TRUS/MRI fusion-guided and/or systematic biopsy. Histopathology results were used as ground truth. The recurrent cancer detection sensitivity of a bpMRI-based AI model, which was developed on a large dataset to primarily identify lesions in treatment naïve patients, was compared to a prospective radiologist assessment using the Wald

Corresponding Author: Baris Turkbey, turkbeyi@mail.nih.gov, Phone: 240-760-6112, Address: Molecular Imaging Branch. National Cancer Institute, National Institutes of Health, 10 Center Dr., MSC 1182, Building 10, Room B3B85, Bethesda, MD 20892.

*Authors share senior co-authorship

test. Subanalysis was conducted on patients stratified by the treatment modality (external beam radiation treatment [EBRT] and brachytherapy) and the prostate volume quartiles.

Results: Of the 62 patients included (median age = 70 years; median PSA = 3.51 ng/ml; median prostate volume = 27.55 ml), 56 recurrent PCa foci were identified within 46 patients. The AI model detected 40 lesions in 35 patients. The AI model performance was lower than the prospective radiology interpretation (Rad) on a patient-(AI: 76.1% vs. Rad: 91.3%, p =0.02) and lesion-level (AI: 71.4% vs. Rad: 87.5%, p =0.01). The mean number of false positives per patient was 0.35 (range: 0-2). The AI model performance was higher in EBRT group both on patient-level (EBRT: 81.5% [22/27] vs. brachytherapy: 68.4% [13/19]) and lesion-level (EBRT: 79.4% [27/34] vs. brachytherapy: 59.1% [13/22]). In patients with gland volumes >34 ml (n=25), detection sensitivities were 100% (11/11) and 94.1% (16/17) on patient-and lesion-level, respectively.

Conclusion: The reported bpMRI-based AI model detected the majority of locally recurrent prostate cancer after radiotherapy. Further testing including external validation of this model is warranted prior to clinical implementation.

Keywords

prostate cancer; radiotherapy; biochemical recurrence; MRI; artificial intelligence

Introduction

Prostate cancer (PCa) is among the leading causes of cancer mortality in the US (1). Treatment approaches such as radiation therapy and surgery are the main curative approaches offered to patients with localized PCa. Radiation therapy options mainly include external beam radiation therapy (EBRT) and brachytherapy, in which the radiation is delivered to the gland with either temporary (high dose rate [HDR]) or permanent (low dose rate [LDR]) implantation of radiation sources (2). Despite the promising success rates of radiation therapy, approximately 15% of intermediate and high risk patients who receive definitive radiotherapy may develop biochemical recurrence (BCR) within 5 years (3–5). Biochemical failure may result from local or metastatic recurrence either in isolation or in combination.

In the setting of post-radiotherapy, BCR is defined by the Phoenix criteria or an elevation of ≥2 ng/ml from the nadir prostate-specific antigen (PSA) level (6). Repeated rises in PSA after definitive radiotherapy usually prompts evaluation with advanced imaging techniques such as multiparametric MRI (mpMRI) (7,8) and PET/CT with novel tracers such as ^{18}F-fluciclovine (Axumin®) or PSMA-targeted PET agents (9). The role of T2-weighted imaging (T2WI) imaging is limited in PCa recurrence, as the whole gland appears diffusely hypointense following radiation therapy (10). On the other hand, malignant tissue is characterized by early contrast enhancement on dynamic contrast enhanced (DCE) MRI, hyperintense appearance on high b-value diffusion weighted imaging (DWI) and hypointense signal intensity on apparent diffusion coefficient [ADC] map) (11,12). However, local recurrence of PCa may remain occult due to the subtlety of these imaging findings.

Although the use of machine learning and deep learning-based artificial intelligence (AI) models for PCa detection is well studied in treatment-naïve PCa patients (13,14), the automated detection of radiorecurrent PCa remains understudied. An AI-based approach to assist in this setting is crucial since MRI evaluations in BCR patients are more difficult and prone to inter-reader variability resultant from treatment-associated changes to the prostate and surrounding tissues (15). Automated identification of recurrent PCa foci without DCE MRI may not only allow early intervention (16) but also prevent potential problems arising from contrast, including safety risks and financial burdens. In the setting of post-radiotherapy imaging, the integrity and shape of the prostate gland are preserved and recurrent cancer imaging features on bpMRI can be quite similar to those of treatment-naïve localized prostate cancer. We hypothesized that a bpMRI-based AI model, which was trained on a large, diverse dataset to identify lesions in treatment-naïve patients, could potentially identify prostate cancer recurrence in patients with BCR after definitive radiotherapy (EBRT or brachytherapy), and assist radiologists in image interpretation.

Materials and Methods

Study Population

This is a single center, HIPAA compliant, retrospective study conducted on patients who were enrolled on institutional review board approved clinical protocols (NCT01834001, NCT03181867, NCT03354416). All patients in the study provided informed, written consent for research studies employing prostate MRI as part of their diagnostic or staging evaluation prior to biopsy. We identified patients with BCR after radiation therapy (EBRT or brachytherapy) who underwent MRI and subsequent MRI/US fusion-guided and/or systematic biopsy at our institution between January 2015 and October 2022. Exclusion criteria included prior accompanying prostate cancer treatment (i.e., radical prostatectomy, focal therapy) and AI-processing errors due to image quality. In addition to details regarding the initial technique of radiotherapy, demographic information such as age, race, clinical characteristics (PSA, prostate volume), biopsy technique, and pathological findings at biopsy were collected from the medical records (Table 1).

Image Acquisition and Evaluation

All patients underwent imaging with a 3T scanner (Ingenia Elition; Philips Healthcare, Best, the Netherlands or Achieva; Philips Healthcare, Best, the Netherlands or Verio; Siemens Healthcare, Erlangen, Germany). Images were acquired using a surface coil (n=62, SENSE, Philips Healthcare, Best, the Netherlands) in isolation or in combination with an endorectal coil (n=38, BPX-30, Medrad, Pittsburgh, PA). Further details regarding image acquisition and technical parameters are presented in the supplemental materials (Supplemental Table 1–2).

All MRI interpretations were prospectively conducted by a genitourinary radiologist with more than 15 years of experience in prostate imaging (~1000 scans/year). All mpMRI sequences (T2WI, high b-value DWI, ADC map, and DCE) were utilized by the radiologist during prostate MRI reads. The same radiologist prospectively contoured both the whole

gland and intraprostatic lesions for MRI/US fusion-guided biopsy procedures using a commercial software (DynaCAD, Philips).

Prostate Biopsy Procedure

All patients underwent subsequent targeted (MRI/US fusion-guided biopsy) and/or systematic biopsy via a transrectal or transperineal approach. Biopsies were performed by either a urologist (>15 years of experience in MRI/US fusion-guided biopsy) or an interventional radiologist (19 years of experience in MRI/US fusion-guided biopsy) using a commercial biopsy system (UroNav, Philips, Gainesville, FL, USA). Biopsy cores underwent histopathological assessment by an expert pathologist (>15 years of experience in genitourinary pathology).

AI-assisted Radiologist Retrospective Readouts on bpMRI

A previously developed bpMRI-based AI model was used for PCa detection in this study (17). After a washout period of ≥9 months, the same genitourinary radiologist who prospectively performed the initial clinical readouts on mpMRI, conducted another interpretation session on bpMRIs with AI assistance using a first-reading paradigm (18). The process involved showing the radiologist AI-generated binary and probability prediction maps first, followed by displaying the conventional bpMRI sequences. During this process, the radiologist was limited to either accepting or rejecting the AI-generated lesion predictions. As per the first-reader paradigm (19,20), the radiologist was not allowed to identify any additional lesions beyond the ones predicted by the AI.

AI Evaluation and Statistical Analysis

The performance of the AI model was evaluated both on a patient and lesion level. Histopathological reports of MRI-guided targeted and systematic biopsies were used as ground truth (Supplemental Figure 1). If the SBx did not align with the TBx and detected cancer in an area where TBx did not, the corresponding SBx sector was considered a separate cancerous focus. Moreover, if multiple SBx sectors were involved without corresponding positivity on TBx and they were not adjacent to each other, they were treated as separate foci as well. In the lesion-level analysis, each prediction of the AI algorithm which corresponded to a cancerous focus on histopathology was considered a true positive (TP). The remainder of the AI-predicted lesions which do not overlap with cancer-positive targeted biopsy lesion contours or do not correspond to a cancer-positive region on systematic sextant biopsy were counted as false positives (FP). Pathologically confirmed cancerous foci which were not predicted by the AI model were deemed as false negatives (FN). As the ground truth was based on biopsy outcomes rather than surgical samples, the true negatives were not assessed in the lesion-level analysis. On a patient-level, at least one true AI prediction was considered as a true positive, whereas any AI prediction on a patient without cancer was considered a false positive. For the scans without any AI-predicted lesions, patients who had cancer on the biopsy were considered false negative, and patients without any evidence of cancer were considered true negative (TN).

For cancer detection sensitivity at lesion- and patient-level, 95% confidence intervals (CI) and standard deviations were estimated from n=2000 bootstrapped samples by random

sampling with replacement on the patient level using R software (version 4.1.2; R Foundation for Statistical Computing, Vienna, Austria). The Wald test was then used to compare the sensitivity and positive predictive value of the standalone AI model, unassisted and assisted radiologist reads for cancer detection. Descriptive statistics were used to summarize the performance metrics of the AI algorithm on subgroups (stratified by treatment technique and prostate volume). On patient-level, Wilcoxon rank-sum test was performed to assess the association between prostate volume and AI recurrence detection. Failure analysis was conducted to determine the false positive and false negative distribution. All p-values were two-sided and a $p < 0.05$ was considered statistically significant.

Results

Patient Characteristics

A total of 66 patients with a prior history of radiation treatment who received a prostate MRI examination and underwent biopsy at our institution between January 2015 and October 2022 were identified. Patients who underwent prostatectomy before (n=2) or received focal therapy (n=1) in addition to radiation treatment prior to imaging were excluded. Additionally, one patient (n=1) was excluded from the analysis due to poor image quality and AI processing error. The final study sample consisted of 62 patients who were previously treated with EBRT (n=36) or LDR brachytherapy (n=26) (Figure 1). The median age of the cohort was 70 years (interquartile range [IQR]: 65-75 years). More than half of the patients were Caucasian (n=48), which was followed by African American (n=11), Asian (n=2), and multiracial (n=1) patients. The median PSA level was 3.51 ng/ml (IQR: 1.99-5.42 ng/ml). The median number of days between the imaging and biopsy was 38.5 days (IQR: 25-53 days). In the study population, most of the patients (n=46) had biopsy-proven recurrent cancer (subgroup median PSA of 3.51 ng/ml [IQR: 2.06-5.58 ng/ml]). These baseline characteristics are summarized in Table 1.

Lesion-level Analysis

In total, 56 cancerous foci were identified at biopsy in 46 patients. The AI model detected 40 of the biopsy-proven cancerous lesions, achieving a sensitivity of 71.4% (40/56), whereas the radiologist prospectively detected 49 of the biopsy-proven cancerous foci. When compared with the radiologist, the AI model had a lower lesion-level sensitivity (AI: 71.4% [95% CI:58, 83.7] vs. unassisted Rad: 87.5% [95% CI:78, 96.3], p value=0.01) (Figure 2). The total number false positives were similar between the radiologist (n=21) and AI (n=22), as well as the positive predictive value (PPV) (standalone AI: 64.5% [95% CI:53.3, 76.6] vs. unassisted Rad: 70% [95% CI:57.5, 82.2], p value=0.39) The mean number of false positives per patient was 0.35 (median= 0, range= [0,2]). On the other hand, mean number of false negatives per patient was 0.26 (median= 0, range= [0,2]).

Patient-level Analysis

Overall, 46 out of 62 patients were confirmed to harbor an intraprostatic recurrence of prostate cancer after histopathological examination (Table 2). The AI model predicted at least one biopsy-verified lesion in 35 patients and failed to detect cancer in the 11 remaining patients with histologic evidence of local recurrence. Additionally, among patients without

any evidence of malignancy on histopathology (n=16), the AI model incorrectly identified lesion(s) in 7 patients but correctly predicted the absences of recurrent cancerous foci for 9 patients. When compared to the prospective radiology readouts, the performance of the AI model for recurrent PCa detection was lower (standalone AI: 76.1% [95% CI:63.8, 87.8] vs. unassisted Rad: 91.3% [95% CI:82.6, 98.0]) with a p value of 0.02 (Figure 2).

Impact of Radiotherapy Technique on AI Model Performance

More than half of the patients (n=36) were treated with external beam radiation therapy (EBRT). In the EBRT treated patients, a total of 34 cancer foci were found in 27 patients. An example of a post-EBRT recurrence is shown in Figure 3. The AI model was able to detect 27 cancer foci (lesion-level sensitivity: 79.4% [27/34]) among 22 patients (patient-level sensitivity: 81.5% [22/27]). The mean number of FPs per patient was 0.36 (median= 0, range= [0,2]), and the mean number of FNs per patient was 0.19 (median=0, range= [0,1]). In the prospective mpMRI reads, 47 lesions were identified and 32 of them were histopathologically verified as recurrent PCa (lesion level sensitivity: 94.1% [32/34]).

Among patients with brachytherapy history (n=26), 19 were diagnosed with recurrent PCa and had 22 cancer foci. The AI model was able to detect only 13 lesions in 13 patients achieving a lesion level sensitivity of 59.1% (13/22) and patient level sensitivity of 68.4% (13/19). Mean number of FPs per patient was slightly lower than EBRT patients with a value of 0.34 (median= 0, range= [0,2]). However, the mean number of FNs per patient was higher for the brachytherapy subgroup (mean=0.34, median= 0, range= [0,2]) when compared to the EBRT subgroup (mean=0.19, median= 0, range= [0,2]). The radiologist detected 17 of 22 cancerous foci with 6 accompanying false predictions at mpMRI, achieving a lesion level sensitivity of 77.3%.

The Impact of Prostate Volume on AI Model Performance

The median prostate volume was 27.55 ml with an IQR range of 21-34 ml in our patients. Patients were divided into 4 subgroups: based on quartile values of the study sample: ≤ 21ml, 21-27.55ml, 27.55-34ml, and >34ml (Figure 4). Patients whose recurrent diseases were correctly identified by the AI were more likely to have larger glands when compared to the ones which were missed by the AI ($p = 0.03$). For patients with prostate volumes greater than 34ml (n=15), the lesion-level and patient-level sensitivities were 94.1% (16/17) and 100% (11/11), respectively. Contrastingly, for patients with gland sizes less than or equal to 21 ml (n=18), the lesion-level and patient-level sensitivities were only 57.1% (8/14) and 66.7% (8/12), respectively.

Comparison of AI-assisted Readouts with Standalone AI and Prospective mpMRI Reads

In AI-assisted readouts, the reader rejected 11 predictions made by the AI and agreed with the other 51 predictions. Out of 51 predictions, 40 were positive for recurrent cancer. Both the AI-assisted readouts and standalone AI had the same lesion-level and patient-level sensitivity for recurrence detection, however, the PPV of the AI-assisted read was higher than that of standalone AI (AI-assisted Rad: 78.4% [95% CI:67.6, 88.9] vs. standalone AI: 64.5% [95% CI:53.3, 76.6]) with a p value <0.001. Moreover, the PPV of the AI-assisted read was moderately improved to the unassisted, prospective read (AI-assisted Rad: 78.4%

[95% CI:67.6, 88.9] vs. unassisted Rad: 70% [95% CI:57.5, 82.2]), though not statistically significant (p value=0.14).

Standalone AI model Failure Analysis

False positive analysis: A total of 22 FP predictions were made by the standalone AI model (Figure 5). Among patients with FP predictions (n=19), the majority occurred in patients treated with EBRT (n=12), with 7 occurring in patients who had received brachytherapy. More than half of the FPs were found in the transition zone (54.5% [12/22]) (Figure 6). Regarding the craniocaudal distribution of FPs, half the FPs were observed within the mid-gland (50%, [11/22]). Of the other half, 8 were in apex and only 3 FPs were located at the base of the prostate. In terms of laterality, no predilection was noted for either side as 8 FPs were observed in each hemigland (both right and left 36.4% [8/22]) with the remainder occurring in the midline (27.2% [6/22]). Only a third of the FPs were situated anteriorly (36.4%, [8/22]).

False negative analysis: In total, there were 16 cancer foci found in 13 patients which were not detected by the standalone AI model (Figure 7). Nine FNs were observed in the brachytherapy subgroup (n=6 patients), whereas 7 FNs were observed in the EBRT subgroup (n=7 patients). Unlike FPs, most of the FNs were located in the peripheral zone (81.3%, [13/16]). The majority of FNs were situated in the prostate base (37.5%, [6/16]) and mid-gland (37.5%, [6/16])) (Figure 8). FNs were most commonly lateralized to the left (56.3% [9/16]). The remainder of the FNs were right sided (37.5% [6/16]) with exception of a single FN occurring in the midline. Moreover, all FNs except one were found in the posterior gland (93.8%, [15/16]).

Discussion

Prostate cancer recurrence remains as a concern despite advances in localized prostate cancer management. Imaging plays a key role in timely identification of local and distal relapse after curative treatment. In our study, we evaluated the performance of an AI model, which was trained on a diverse, multi-institutional dataset without DCE, to detect prostate cancer local recurrence in patients with an intact prostate after an initial course of curative radiotherapy. The majority of patients with recurrent prostate cancer were correctly identified with a biparametric MRI (T2WI & DWI/ADC map)-based AI model which demonstrated a patient-level sensitivity of 76.1% and lesion-level sensitivity of 71.4%. The model detection performance was best amongst patients with larger glands and those in the EBRT subgroup. The radiologist interaction with AI may decrease the number of false positive calls without compromising the model’s detection performance.

Owing to increasing availability and the wide recognition of mpMRI as a prostate imaging modality, patients are increasingly offered imaging at the time of initial diagnosis and at recurrence. Concerns regarding contrast utilization exist due to safety issues, higher economic burden, and longer image acquisition times (21). Except for some studies with small sample sizes suggesting otherwise (22–24), DCE has a crucial role in imaging of recurrent prostate cancer. In a recently proposed guideline, PI-RR, the utilization of DCE is recommended in the evaluation of local recurrence among patients with biochemical

recurrence who have received radiation therapy (25). Although our findings are preliminary, they suggest that an end-to-end, bpMRI-based AI may detect and localize most of the local recurrences following an initial course of radiotherapy without requiring one of the essential components of mpMRI, DCE. Such an AI-based approach can also aid in addressing aforementioned concerns associated with contrast injection. Moreover, avoiding contrast injection with the application of this bpMRI-based AI-detection algorithm could render more frequent, routine imaging a viable strategy in the post-radiotherapy surveillance. This may serve as a companion to PSA monitoring to possibly allow for early detection and intervention for the subgroup of patients with locally recurrent prostate cancer.

Prostate MRI interpretation in primary cancer detection has a steep-learning curve (26), and the assessment of localized cancer recurrence is even more challenging on a posttreatment mpMRI, due to treatment-related global signal changes in the gland. Examples of this include the diffuse hypointense appearance of the prostate on T2WI and lower ADC values of the benign tissue compared to pretreatment state attributed to the decreased cellularity and vascularity in response to radiotherapy (7,27). The AI model detected 35 out of 46 patients with biopsy proven local recurrence without utilizing DCE. Although the lesion detection sensitivity was not as high as an expert radiologist using DCE, the algorithm detected 71.4% of cancerous foci with a relatively small number of false positives (mean number of FPs per patient=0.35). Employment of such an AI model in clinical practice may be particularly useful for novice readers who may not be familiar with prostate cancer recurrence imaging to improve their diagnostic accuracy.

Although the FP rate in brachytherapy patients was slightly lower than that of EBRT patients, the higher FN rate in brachytherapy patients suggests that the AI model was less likely to call out lesions in this subgroup. This lower local recurrence detection performance of AI in brachytherapy patients could be attributed to the distortions on the mpMRI (particularly high b-value DWI) arising from the permanent brachytherapy seeds. In a standard radiology read, DCE is often the only sequence which may identify a local recurrence in LDR brachytherapy patients as T2WI and high b-value DWI are either nondiagnostic or unremarkable. Bearing in mind that the AI model did not utilize DCE, a patient-level sensitivity of 68.4% is still promising. However, additional algorithmic improvements in performance are necessary to improve performance to clinically acceptable levels.

It should be kept in mind that both treatment techniques mentioned in our study cause substantial reduction in gland volume (28). The median prostate volume of our study sample (27.55 ml) was relatively lower than that of the dataset used to train the AI model, which was 60 ml (17). Underrepresentation of smaller glands in the training dataset might explain the relative low performance of AI in prostates with lower volumes. There is also the possibility that a patient with a more preserved gland volume may have a more apparent lesion with a larger tumor-to-gland ratio on MRI. It is worth noting that we have observed better detection performance of AI in EBRT patients, and their median gland volume (30.35 ml) was higher than patients who received brachytherapy (25.5 ml). Thus, rather than a direct association between the prostate size and AI detection rate, the technique of treatment could be the primary factor impacting both the AI model performance and the gland size.

Our failure analysis revealed that FP occurrences were mostly dispersed within the prostate, and they were more commonly observed in the mid-gland and transition zone. Overall, one in every 3 patients had a false positive prediction, which is relatively lower than the reported rates of the other prostate cancer detection algorithms in the literature (29,30). Apart from the impact of the integrated BPH-reduction step in AI model's framework (17), the diffuse hypointense appearance of treated prostate glands may have resulted in a relatively low rate of FPs with an acceptable sensitivity level. In a prior study, the same AI model had a mean sensitivity of 96.1% on patient-level with a mean of 0.44 FPs per patient on a treatment-naïve study sample (17). As the AI model used in our study was originally intended to detect prostate cancer foci in treatment-naïve patients, a different probability threshold may have served to optimize the sensitivity of algorithmic detection in this clinical setting, which in turn may have also led to a higher FP rate. Alternatively, human interaction with AI may also decrease the FP rate as demonstrated in our study.

It is also worth noting that the AI model used in the study is completely blinded to past medical prostate cancer history including baseline PCa location at previous MRI, histopathology, serum PSA. This is in contrast with a prospective mpMRI read, where the radiologist often has access to such information through prior imaging records or clinical reports. It has been shown that local prostate recurrence mostly originates from the site of primary cancer (31), which likely impacts the assessment of the radiologist. As certain clinical parameters such as PSA (32), radiation dose (33,34), androgen deprivation therapy exposure (35) , or MRI features are predictive of disease recurrence following treatment (36,37), one of the next steps towards improving the AI model's prediction could be the utilization of prior imaging (i.e., MRI or PET/CT), details of prior therapy (i.e., radiation dose, technique, or androgen deprivation therapy), or other clinical parameters (i.e., serial PSA measurements or latency of relapse).

Our study had several limitations. First, the study sample size was relatively small. As we aimed to correlate the AI predictions with histopathology, our study sample was restricted to patients who underwent mpMRI and subsequent biopsy at our institution. Our findings need to be validated on a larger sample, which may be possible with multi-institutional efforts. Second, the AI model used in our study automatically filters out predictions outside the prostate segmentation. Therefore, tumors located in the seminal vesicles cannot be detected with this AI model. Third, not all patients underwent combined targeted and systematic biopsy as some patients had no radiographically detected focus of recurrent tumor noted by the interpreting human radiologist at time of pre-biopsy diagnostic workup. In patients who did not undergo systematic biopsy, we considered AI predictions outside the targeted biopsy region as false positives, which might have inflated the false positive rates by the AI model. Fourth, as the pathological confirmation in our study relied on TBx and SBx, the total disease burden may not have been truly assessed as it would have been in whole-mount specimens, resulting in high sensitivity rates by both the AI and radiologist. Fifth, we were unable to gauge the effect of AI on the time taken for image interpretation, as the prospective evaluations were conducted in a clinical setting without tracking the reporting duration. Sixth, the same genitourinary radiologist conducted the AI-assisted readouts; ideally, having multiple readers would better demonstrate the impact of AI-assistance in recurrence detection. Additionally, our study did not include PI-RR evaluations since the

PI-RR system had not been published when the prospective readouts of this study population were conducted. Finally, prospective reads were performed by an expert genitourinary radiologist, which may have resulted in an artificially large performance difference between the AI model and the clinical mpMRI evaluations. Considering this, the AI model may currently have an optimal use case in assisting non-expert radiologists who are challenged to interpret prostate MRIs of patients with biochemically recurrent prostate cancer under investigation for local recurrence.

In conclusion, a deep learning-based AI algorithm was able to identify a considerable proportion of local recurrences on biparametric MRI in prostate cancer patients who had biochemical recurrence after radiation therapy. However, our findings are preliminary and further evaluation in a large, prospective dataset, preferably acquired from multiple institutions, is required to validate our results.

Supplementary Material

Refer to Web version on PubMed Central for supplementary material.

Acknowledgments

Enis C. Yilmaz: None

Stephanie A. Harmon: None

Mason J. Belue: None

Katie M. Merriman: None

Tim E. Phelps: None

Yue Lin: None

Charisse Garcia: None

Lindsey Hazen: None

Krishnan R. Patel: None

Maria J. Merino: None

Bradford J. Wood: Principal investigator on cooperative research and development agreement (CRADA) between National Institutes of Health (NIH) and Philips and CRADAs with industry partners unrelated to this work; travel support related to CRADAs; royalties from NIH related to Philips licensing agreement; patents planned, issued, or pending.

Peter L. Choyke: Receives payment from royalties paid to the U.S. government for patents on MRI US fusion biopsy licensed to Philips Medical.

Peter A. Pinto: Institutional CRADA with Philips; royalties from NIH related to Philips licensing agreement; NIH-related patents planned, issued, or pending (U.S. patent nos. 8 447 384 and 10 215 830).

Deborah E. Citrin: None

Baris Turkbey: CRADAs with NVIDIA and Philips; royalties from NIH; patents planned, issued, or pending in the field of artificial intelligence.

References

1. Siegel RL, Miller KD, Fuchs HE, Jemal A. Cancer statistics, 2022. CA Cancer J Clin. 2022 Jan;72(1):7–33. [PubMed: 35020204]
2. Litwin MS, Tan HJ. The Diagnosis and Treatment of Prostate Cancer: A Review. JAMA. 2017 Jun 27;317(24):2532–42. [PubMed: 28655021]
3. Krauss DJ, Karrison TG, Martinez AA, Morton G, Yan D, Bruner DW, et al. Dose Escalated Radiotherapy Alone or in Combination With Short-Term Androgen Suppression for Intermediate Risk Prostate Cancer: Outcomes From the NRG Oncology/RTOG 0815 Randomized Trial. International Journal of Radiation Oncology, Biology, Physics. 2021 Nov 1;111(3):S1.
4. Kerkmeijer LGW, Groen VH, Pos FJ, Haustermans K, Monninkhof EM, Smeenk RJ, et al. Focal Boost to the Intraprostatic Tumor in External Beam Radiotherapy for Patients With Localized Prostate Cancer: Results From the FLAME Randomized Phase III Trial. JCO. 2021 Mar;39(7):787–96.
5. Nabid A, Carrier N, Martin AG, Bahary JP, Lemaire C, Vass S, et al. Duration of Androgen Deprivation Therapy in High-risk Prostate Cancer: A Randomized Phase III Trial. Eur Urol. Oct 2018 1;74(4):432–41. [PubMed: 29980331]
6. Roach M, Hanks G, Thames H, Schellhammer P, Shipley WU, Sokol GH, et al. Defining biochemical failure following radiotherapy with or without hormonal therapy in men with clinically localized prostate cancer: recommendations of the RTOG-ASTRO Phoenix Consensus Conference. Int J Radiat Oncol Biol Phys. 2006 Jul 15;65(4):965–74. [PubMed: 16798415]
7. Mertan FV, Greer MD, Borofsky S, Kabakus IM, Merino Maria J, Wood BJ, et al. Multi-parametric Magnetic Resonance Imaging of Recurrent Prostate Cancer. Top Magn Reson Imaging. 2016 Jun;25(3):139–47. [PubMed: 27187164]
8. Valle LF, Greer MD, Shih JH, Barrett T, Law YM, Rosenkrantz AB, et al. Multiparametric MRI for the detection of local recurrence of prostate cancer in the setting of biochemical recurrence after low dose rate brachytherapy. Diagn Interv Radiol. 2018 Jan;24(1):46–53. [PubMed: 29317377]
9. Lindenberg ML, Turkbey B, Mena E, Choyke PL. Imaging Locally Advanced, Recurrent, and Metastatic Prostate Cancer: A Review. JAMA Oncol. 2017 Oct 1;3(10):1415–22. [PubMed: 28097325]
10. Rouvière O, Valette O, Grivolat S, Colin-Pangaud C, Bouvier R, Chapelon JY, et al. Recurrent prostate cancer after external beam radiotherapy: value of contrast-enhanced dynamic MRI in localizing intraprostatic tumor--correlation with biopsy findings. Urology. 2004 May;63(5):922–7. [PubMed: 15134982]
11. Kim CK, Park BK, Lee HM. Prediction of locally recurrent prostate cancer after radiation therapy: incremental value of 3T diffusion-weighted MRI. J Magn Reson Imaging. 2009 Feb;29(2):391–7. [PubMed: 19161194]
12. Kim CK, Park BK, Park W, Kim SS. Prostate MR imaging at 3T using a phased-arrayed coil in predicting locally recurrent prostate cancer after radiation therapy: preliminary experience. Abdom Imaging. 2010 Apr 1;35(2):246–52. [PubMed: 19130116]
13. Syer T, Mehta P, Antonelli M, Mallett S, Atkinson D, Ourselin S, et al. Artificial Intelligence Compared to Radiologists for the Initial Diagnosis of Prostate Cancer on Magnetic Resonance Imaging: A Systematic Review and Recommendations for Future Studies. Cancers (Basel). 2021 Jul 1;13(13):3318. [PubMed: 34282762]
14. Twilt JJ, van Leeuwen KG, Huisman HJ, Fütterer JJ, de Rooij M. Artificial Intelligence Based Algorithms for Prostate Cancer Classification and Detection on Magnetic Resonance Imaging: A Narrative Review. Diagnostics (Basel). 2021 May 26;11(6):959. [PubMed: 34073627]
15. Patel P, Mathew MS, Trilisky I, Oto A. Multiparametric MR Imaging of the Prostate after Treatment of Prostate Cancer. Radiographics. 2018;38(2):437–49. [PubMed: 29373089]
16. Cornford P, van den Bergh RCN, Briers E, Van den Broeck T, Cumberbatch MG, De Santis M, et al. EAU-EANM-ESTRO-ESUR-SIOG Guidelines on Prostate Cancer. Part II-2020 Update: Treatment of Relapsing and Metastatic Prostate Cancer. Eur Urol. 2021 Feb;79(2):263–82. [PubMed: 33039206]

17. Mehralivand S, Yang D, Harmon SA, Xu D, Xu Z, Roth H, et al. A Cascaded Deep Learning-Based Artificial Intelligence Algorithm for Automated Lesion Detection and Classification on Biparametric Prostate Magnetic Resonance Imaging. Acad Radiol. 2022 Aug;29(8):1159–68. [PubMed: 34598869]

18. Beyer F, Zierott L, Fallenberg EM, Juergens KU, Stoeckel J, Heindel W, et al. Comparison of sensitivity and reading time for the use of computer-aided detection (CAD) of pulmonary nodules at MDCT as concurrent or second reader. Eur Radiol. 2007 Nov 1;17(11):2941–7. [PubMed: 17929026]

19. Greer MD, Lay N, Shih JH, Barrett T, Bittencourt LK, Borofsky S, et al. Computer-aided diagnosis prior to conventional interpretation of prostate mpMRI: an international multireader study. Eur Radiol. 2018 Oct;28(10):4407–17. [PubMed: 29651763]

20. Gaur S, Lay N, Harmon SA, Doddakashi S, Mehralivand S, Argun B, et al. Can computer-aided diagnosis assist in the identification of prostate cancer on prostate MRI? a multi-center, multi-reader investigation. Oncotarget. 2018 Sep 18;9(73):33804–17. [PubMed: 30333911]

21. Belue MJ, Yilmaz EC, Daryanani A, Turkbey B. Current Status of Biparametric MRI in Prostate Cancer Diagnosis: Literature Analysis. Life (Basel). 2022 May 28;12(6):804. [PubMed: 35743835]

22. Alonzo F, Melodelima C, Bratan F, Vitry T, Crouzet S, Gelet A, et al. Detection of locally radio-recurrent prostate cancer at multiparametric MRI: Can dynamic contrast-enhanced imaging be omitted? Diagnostic and Interventional Imaging. 2016 Apr 1;97(4):433–41. [PubMed: 26928245]

23. Donati OF, Jung SI, Vargas HA, Gultekin DH, Zheng J, Moskowitz CS, et al. Multiparametric Prostate MR Imaging with T2-weighted, Diffusion-weighted, and Dynamic Contrast-enhanced Sequences: Are All Pulse Sequences Necessary to Detect Locally Recurrent Prostate Cancer after Radiation Therapy? Radiology. 2013 Aug;268(2):440–50. [PubMed: 23481164]

24. Abd-Alazeez M, Ramachandran N, Dikaios N, Ahmed HU, Emberton M, Kirkham A, et al. Multiparametric MRI for detection of radiorecurrent prostate cancer: added value of apparent diffusion coefficient maps and dynamic contrast-enhanced images. Prostate Cancer Prostatic Dis. 2015 Jun;18(2):128–36. [PubMed: 25644248]

25. Panebianco V, Villeirs G, Weinreb JC, Turkbey BI, Margolis DJ, Richenberg J, et al. Prostate Magnetic Resonance Imaging for Local Recurrence Reporting (PI-RR): International Consensus -based Guidelines on Multiparametric Magnetic Resonance Imaging for Prostate Cancer Recurrence after Radiation Therapy and Radical Prostatectomy. Eur Urol Oncol. 2021 Dec;4(6):868–76. [PubMed: 33582104]

26. Rosenkrantz AB, Ayoola A, Hoffman D, Khasgiwala A, Prabhu V, Smereka P, et al. The Learning Curve in Prostate MRI Interpretation: Self-Directed Learning Versus Continual Reader Feedback. American Journal of Roentgenology. 2017 Mar;208(3):W92–100. [PubMed: 28026201]

27. Song I, Kim CK, Park BK, Park W. Assessment of Response to Radiotherapy for Prostate Cancer: Value of Diffusion-Weighted MRI at 3 T. American Journal of Roentgenology. 2010 Jun;194(6):W477–82. [PubMed: 20489065]

28. Gaur S, Turkbey B. Prostate MR Imaging for Posttreatment Evaluation and Recurrence. Urologic Clinics of North America. 2018 Aug 1;45(3):467–79. [PubMed: 30031466]

29. Hosseinzadeh M, Saha A, Brand P, Slootweg I, de Rooij M, Huisman H. Deep learning-assisted prostate cancer detection on bi-parametric MRI: minimum training data size requirements and effect of prior knowledge. Eur Radiol. 2022 Apr;32(4):2224–34. [PubMed: 34786615]

30. Giannini V, Mazzetti S, Armando E, Carabalona S, Russo F, Giacobbe A, et al. Multiparametric magnetic resonance imaging of the prostate with computer-aided detection: experienced observer performance study. Eur Radiol. 2017 Oct 1;27(10):4200–8. [PubMed: 28386721]

31. Pucar D, Hricak H, Shukla-Dave A, Kuroiwa K, Drobnjak M, Eastham J, et al. Clinically significant prostate cancer local recurrence after radiation therapy occurs at the site of primary tumor: magnetic resonance imaging and step-section pathology evidence. Int J Radiat Oncol Biol Phys. 2007 Sep 1;69(1):62–9. [PubMed: 17707266]

32. Grossfeld GD, Latini DM, Lubeck DP, Mehta SS, Carroll PR. Predicting Recurrence After Radical Prostatectomy for Patients With High Risk Prostate Cancer. Journal of Urology. 2003 Jan;169(1):157–63. [PubMed: 12478126]

33. Michalski JM, Moughan J, Purdy J, Bosch W, Bruner DW, Bahary JP, et al. Effect of Standard vs Dose-Escalated Radiation Therapy for Patients With Intermediate-Risk Prostate Cancer: The NRG Oncology RTOG 0126 Randomized Clinical Trial. JAMA Oncol. 2018 Jun 14;4(6):e180039. [PubMed: 29543933]

34. Groen VH, Haustermans K, Pos FJ, Draulans C, Isebaert S, Monninkhof EM, et al. Patterns of Failure Following External Beam Radiotherapy With or Without an Additional Focal Boost in the Randomized Controlled FLAME Trial for Localized Prostate Cancer. Eur Urol. 2022 Sep;82(3):252–7. [PubMed: 34953603]

35. Bolla M, Van Tienhoven G, Warde P, Dubois JB, Mirimanoff RO, Storme G, et al. External irradiation with or without long-term androgen suppression for prostate cancer with high metastatic risk: 10-year results of an EORTC randomised study. Lancet Oncol. 2010 Nov;11(11):1066–73. [PubMed: 20933466]

36. Shiradkar R, Ghose S, Jambor I, Taimen P, Ettala O, Purysko AS, et al. Radiomic features from pretreatment biparametric MRI predict prostate cancer biochemical recurrence: Preliminary findings. J Magn Reson Imaging. 2018 Dec;48(6):1626–36. [PubMed: 29734484]

37. Gnep K, Fargeas A, Gutiérrez-Carvajal RE, Commandeur F, Mathieu R, Ospina JD, et al. Haralick textural features on T2 -weighted MRI are associated with biochemical recurrence following radiotherapy for peripheral zone prostate cancer. J Magn Reson Imaging. 2017 Jan;45(1):103–17. [PubMed: 27345946]

Highlights:

1. Detection of local recurrence in patients with prior radiotherapy is challenging.
2. A bpMRI-based AI model detected most locally radiorecurrent cancers.
3. The AI model performance was comparably better in patients with larger glands.
4. The AI detection rates were higher in external beam radiation therapy group.

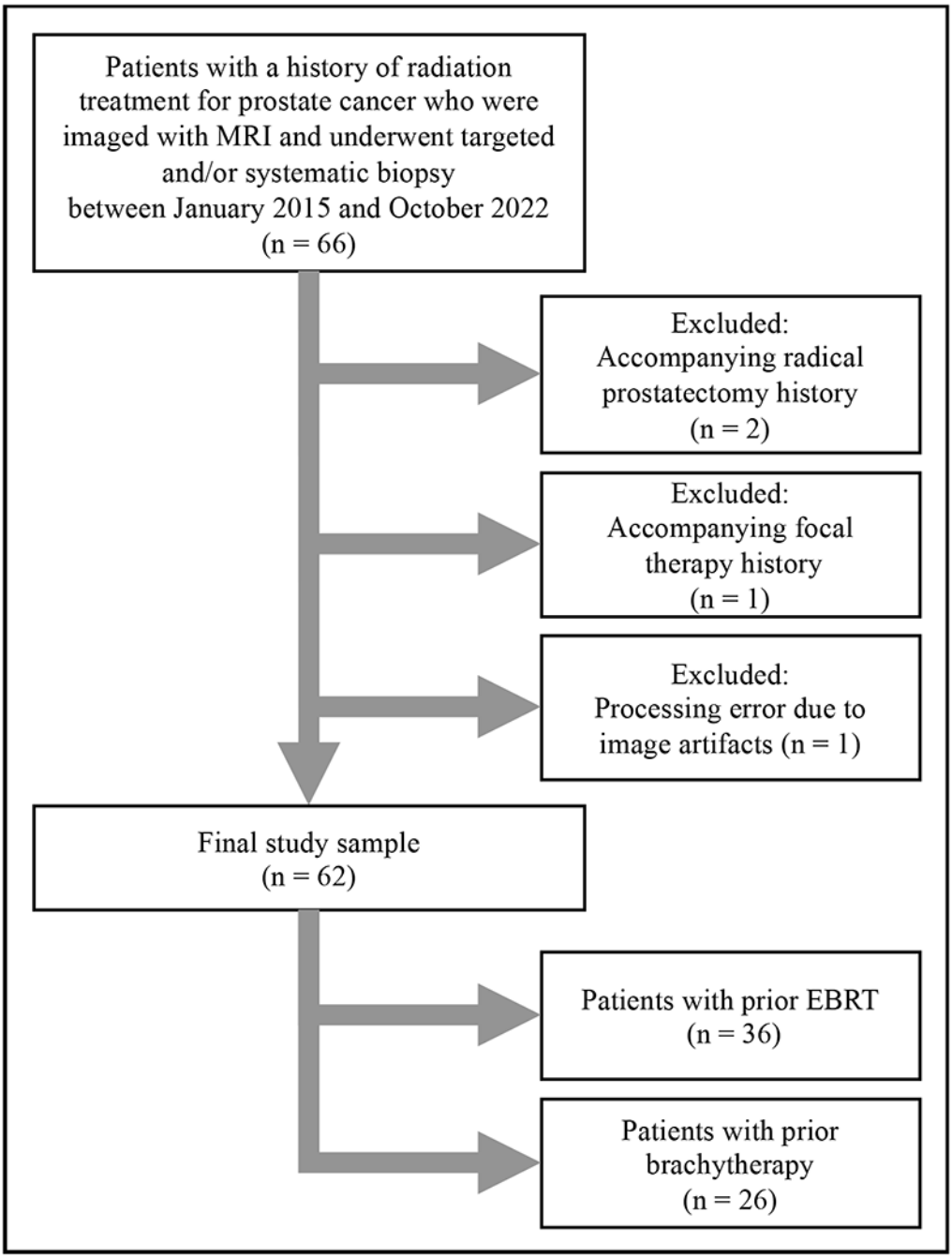

Figure 1.
Study flowchart
EBRT: External beam radiation therapy

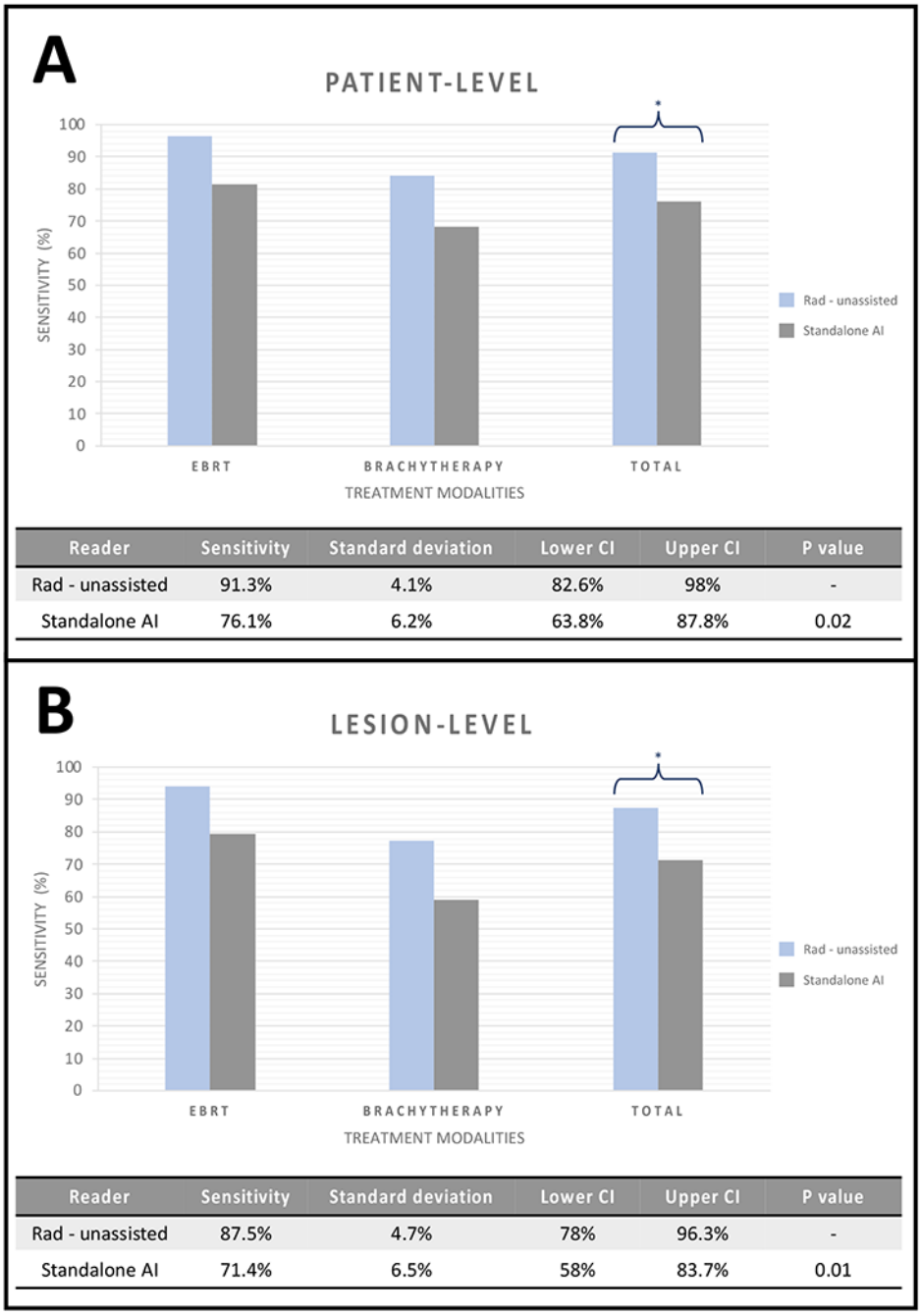

Reader	Sensitivity	Standard deviation	Lower CI	Upper CI	P value
Rad - unassisted	91.3%	4.1%	82.6%	98%	-
Standalone AI	76.1%	6.2%	63.8%	87.8%	0.02

Reader	Sensitivity	Standard deviation	Lower CI	Upper CI	P value
Rad - unassisted	87.5%	4.7%	78%	96.3%	-
Standalone AI	71.4%	6.5%	58%	83.7%	0.01

Figure 2.

Standalone AI and unassisted radiologist readout detection sensitivities on patient-level (A) and lesion-level (B) for both treatment groups combined.

* represents p value of <0.05 for both comparisons.

EBRT: External beam radiation therapy

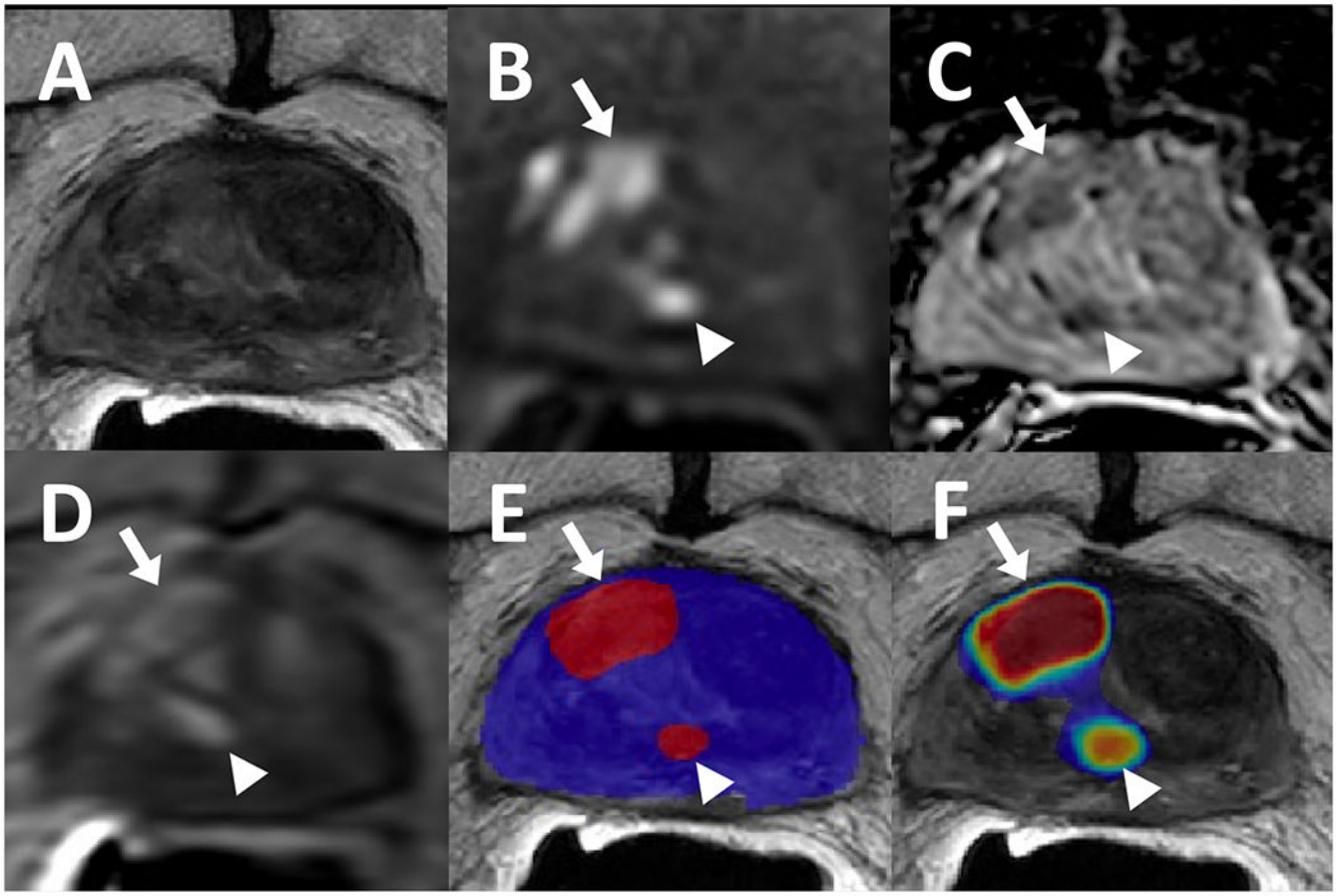

Figure 3.

82-year-old male with a history of external beam radiation therapy for prostate cancer and serum PSA level of 9.33 ng/ml. The patient had lesions in right mid-base anterior transition zone (arrows) and right mid periurethral transition zone (arrowhead) which were visible on T2-weighted imaging (A), ADC map (B), high b-value diffusion weighted imaging (DWI) (C), and dynamic contrast enhancement (DCE) (D). Targeted biopsies obtained from these sites were positive for recurrent cancer, and both were detected by the AI model as displayed in a binary AI prediction map (E) and a probability map (F).

A

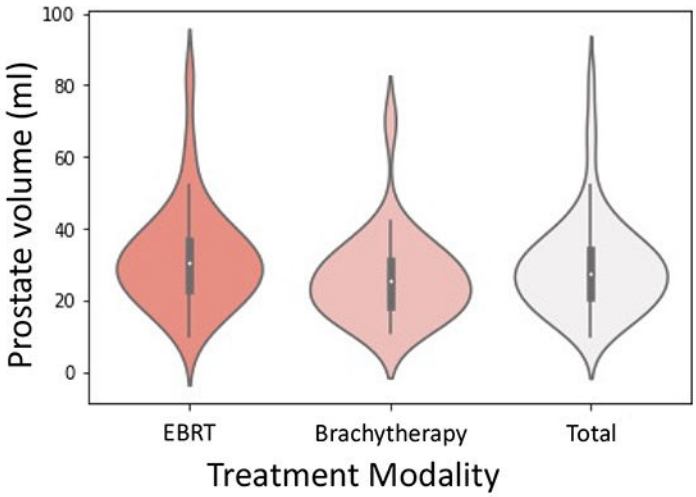

B

		Prostate volume			
		≤ 21 ml	> 21 and ≤ 27.55 ml	> 27.55 and ≤ 34 ml	> 34 ml
EBRT	No. of patients	7	8	11	10
	Patient-level sensitivity	100% (4/4)	50% (3/6)	77.8% (7/9)	100% (8/8)
	Lesion-level sensitivity	100% (4/4)	42.9% (3/7)	77.8% (7/9)	92.9% (13/14)
BRACHY	No. of patients	11	5	5	5
	Patient-level sensitivity	50% (4/8)	75% (3/4)	75% (3/4)	100% (3/3)
	Lesion-level sensitivity	40% (4/10)	60% (3/5)	75% (3/4)	100% (3/3)
TOTAL	No. of patients	18	13	16	15
	Patient-level sensitivity	66.7% (8/12)	60% (6/10)	76.9% (10/13)	100% (11/11)
	Lesion-level sensitivity	57.1% (8/14)	50% (6/12)	76.9% (10/13)	94.1% (16/17)

Figure 4.

Violin plots of prostate volumes in the two treatment modalities (external beam radiation therapy [EBRT] and brachytherapy [Brachy]) (A). Patient- and lesion-level detection sensitivities of standalone AI stratified by prostate volume quartiles (B).

Location	Total FPs (n = 22)
Zone	
Peripheral zone	10 (45.5%)
Transition zone	12 (54.5%)
Regional part	
Base	3 (13.6%)
Mid	11 (50%)
Apex	8 (36.4%)
Side	
Right	8 (36.4%)
Left	8 (36.4%)
Midline	6 (27.3%)
Anterior	
Yes	8 (36.4%)
No	14 (63.6%)

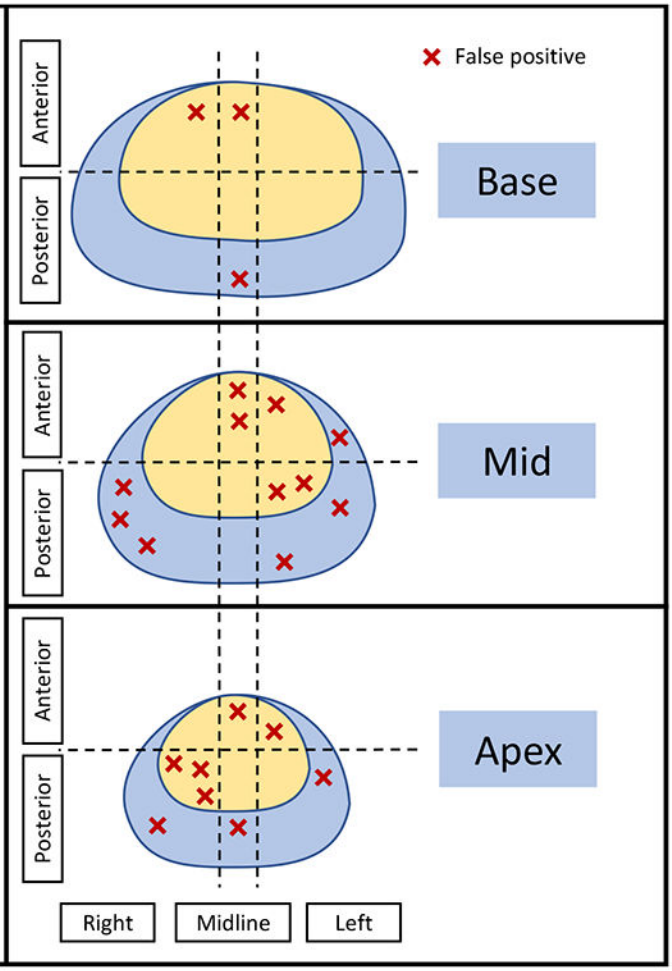

Figure 5.
False-positive distribution of the standalone AI model (red “X” refers to false positively detected lesions by the AI model and their corresponding locations in the prostate sector map)

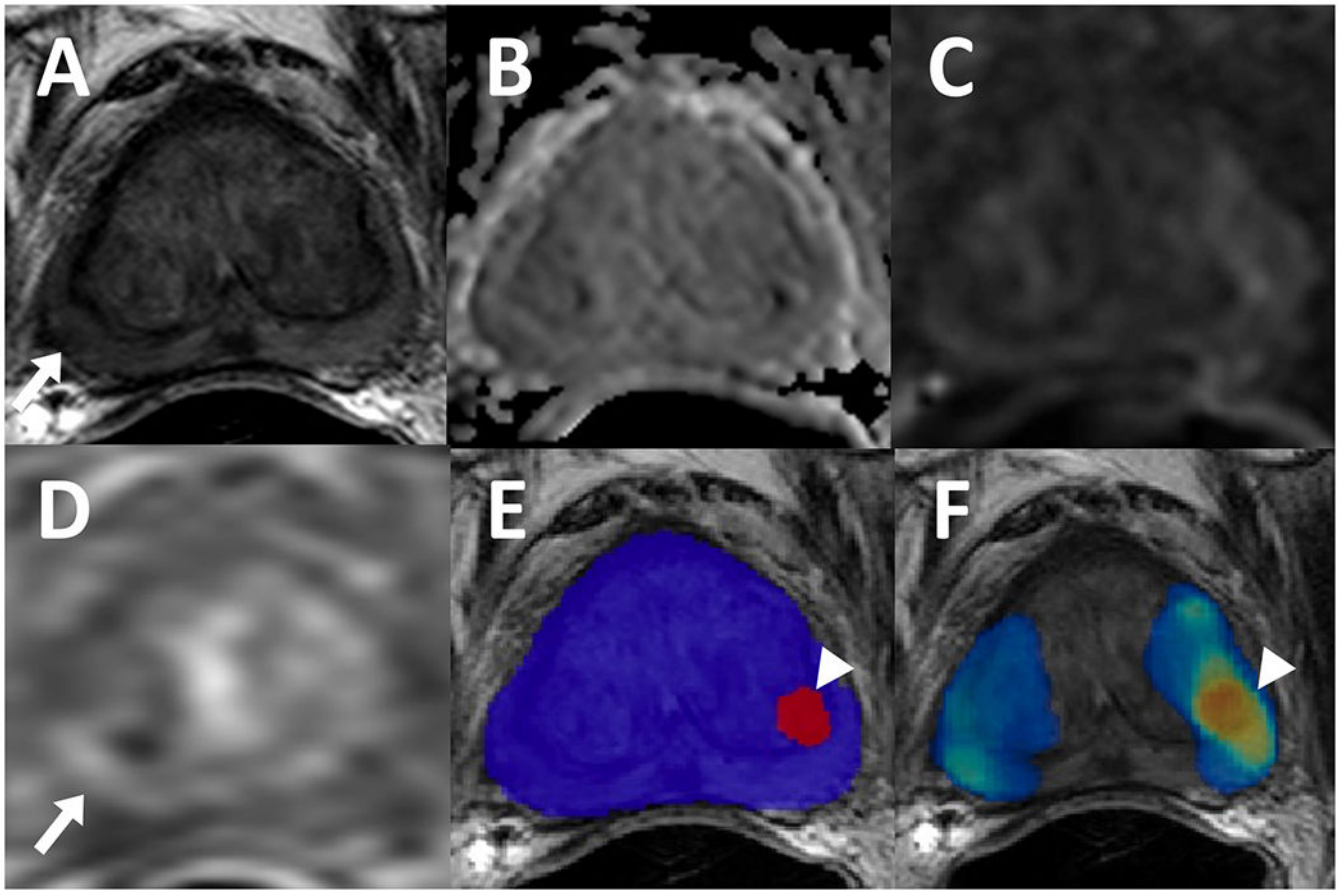

Figure 6.

A 72-year-old male with a history of external beam radiation therapy for prostate cancer and serum PSA level of <0.01 ng/ml. Patient had a lesion in right mid peripheral zone which appears slightly hypointense on T2-weighted imaging (A) (arrow), negative on ADC map (B) and high b-value diffusion weighted imaging (DWI) (C) with a mild focal contrast uptake on dynamic contrast enhancement (DCE) (D) (arrow). Targeted biopsy revealed residual cancer, however, AI model did not detect this lesion. In left mid transition zone, the AI model had a false positive prediction, visible on binary AI prediction map (E) and probability map (F) (arrowhead) which may be attributed to the signal abnormalities caused by an adjacent fiducial marker.

Location	Total FNs (n = 16)
Zone	
Peripheral zone	13 (81.3%)
Transition zone	3 (18.8%)
Regional part	
Base	6 (37.5%)
Mid	6 (37.5%)
Apex	4 (25%)
Side	
Right	6 (37.5%)
Left	9 (56.3%)
Midline	1 (6.3%)
Anterior	
Yes	1 (6.3%)
No	15 (93.8%)

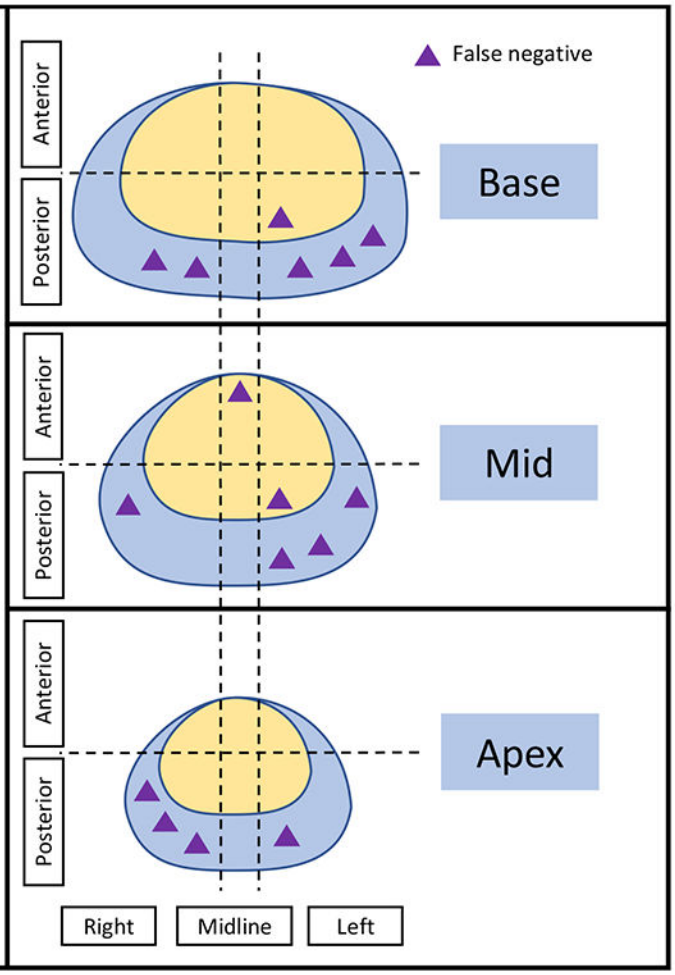

Figure 7.
False-negative distribution of the standalone AI model (purple triangles refer to prostate cancer lesions missed by the AI model and their corresponding locations in the prostate sector map)

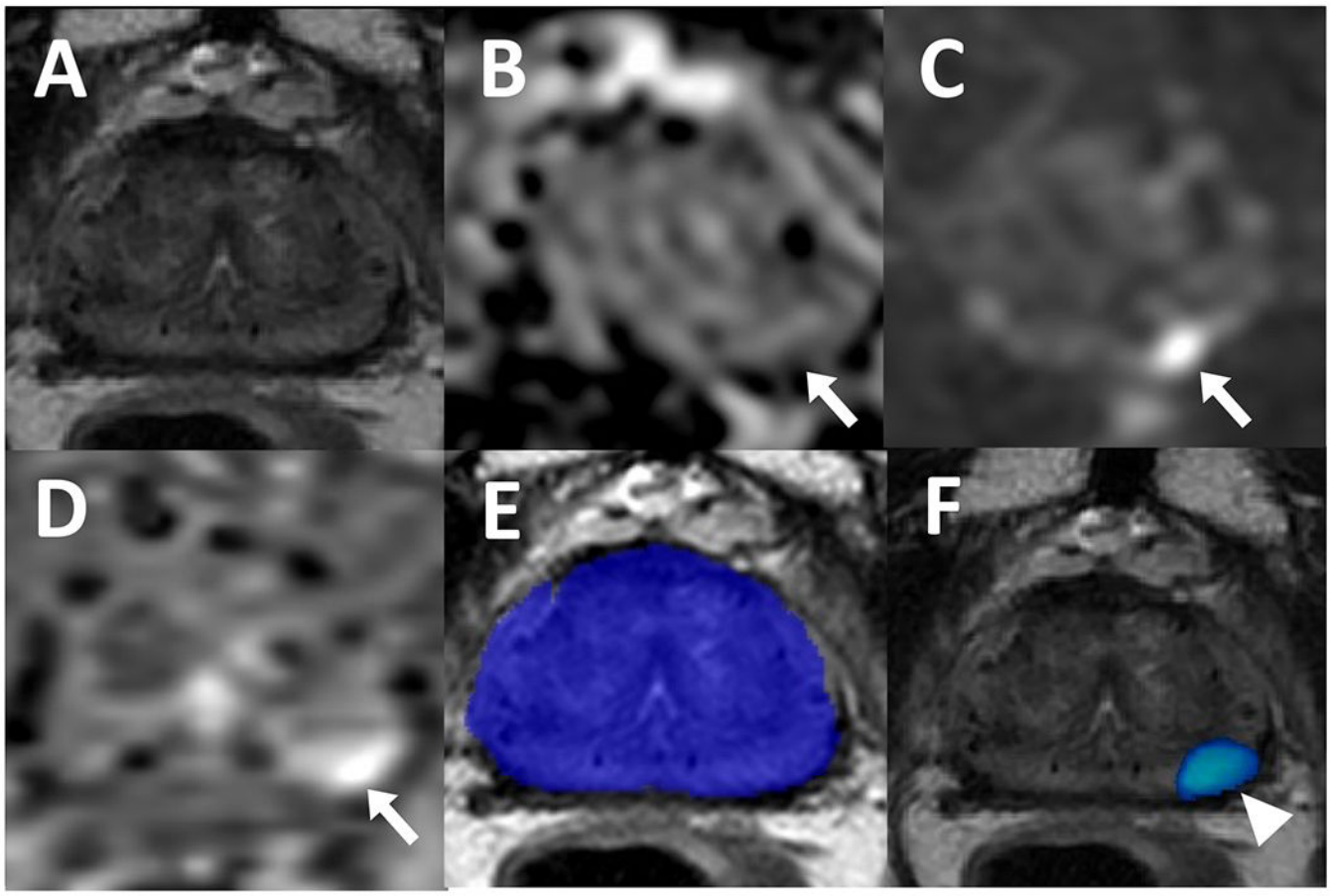

Figure 8.

A 70-year-old male who received brachytherapy for prostate cancer treatment with a serum PSA level of 1.5 ng/ml. Patient has a lesion in left apical-mid peripheral zone which is not visible on T2-weighted imaging (A) but appears hypointense on ADC map (B) and hyperintense on high b-value diffusion weighted imaging (DWI) (C) (arrows). The lesion also demonstrates early enhancement on dynamic contrast enhancement (DCE) (D) (arrow). Recurrent prostate adenocarcinoma was confirmed on targeted biopsy. Biparametric MRI-based AI did not have any prediction on the binary AI prediction map (E) and therefore, this was considered a false negative, however, the probability map (F) localized the cancerous focus (arrowhead).

Table 1 –

Patient Demographics

VARIABLE	DESCRIPTION/UNIT	ALL PATIENTS (N=62)		
		Number of patients (%)	Median	Interquartil e Range (IQR)
AGE	Years		70	65-75
RACE	African American	11 (18)	.	.
	Asian	2 (3)	.	.
	Caucasian	48 (77)	.	.
	Multiracial	1 (2)	.	.
MR-BX INTERVAL	Days	.	38.5	25-53
PSA	ng/ml	.	3.51	1.99-5.42
PROSTATE VOLUME	ml	.	27.55	21-34
BIOPSY SCHEME	Tbx only	10 (16)	.	.
	*Tbx + TR-Sbx	41 (66)	.	.
	Tbx + TP-Sbx	10 (16)	.	.
	TP-Sbx only	1 (2)	.	.
NO. OF CANCEROUS FOCI PER PT.				
	0	16 (26)	.	.
	1	37 (60)	.	.
	2	8 (13)	.	.
	3	1 (2)	.	.

* 4 patients had targeted biopsy only for seminal vesicle lesion

Numbers in parentheses represent percentages

Bx: Biopsy, PSA: Prostate-specific antigen, Tbx: Targeted biopsy, TR-Sbx: Transrectal systematic biopsy, TP-Sbx: Transperineal systematic biopsy

Table 2 –

Overall distribution of recurrent prostate cancer and standalone AI detection sensitivity

Treatment Technique	No. of Pts.	PCa Foci	AI: Lesion-level Sensitivity		PC a Pts.	AI: Patient-level Sensitivity		FPs per patient		FNs per patient	
			Ratio	%		Ratio	%	Mean	Median [range]	Mean	Median [range]
EBRT	36	34	27/34	79.4	27	22/27	81.5	0.36	0 [0, 2]	0.19	0 [0, 1]
BT	26	22	13/22	59.1	19	13/19	68.4	0.34	0 [0, 2]	0.34	0 [0, 2]
Overall	62	56	40/56	71.4	46	35/46	76.1	0.35	0 [0, 2]	0.25	0 [0, 2]

AI: Artificial Intelligence model, BT: Brachytherapy, EBRT: External beam radiation therapy, PCa: Prostate cancer, FP: False positive, FN: False negative.